RESEARCH RELATIVE TO DYNAMIC CHARACTERISTICS OF LINEAR HYDROSTATIC BEARINGS

by

Charles B. Watkins

Iheanyi E. Eronini

and

Howard D. Branch

Department of Mechanical Engineering
Howard University
Washington, D.C. 20059

Final Report

NASA Grant NAG 5-25

October, 1982

ABSTRACT

Vibration of a statically loaded, inherently compensated hydrostatic journal bearing due to oscillating exhaust pressure is investigated. Both angular and radial vibration modes are analyzed. The time-dependent Reynolds equation governing the pressure distribution between the oscillating journal and sleeve is solved together with the journal equation of motion to obtain the response characteristics of the bearing. The Reynolds equation and the equation of motion are simplified by applying regular perturbation theory for small displacements. The numerical solutions of the perturbation equations are obtained by discretizing the pressure field using finite-difference approximations with a modified line-source model which excludes effects due to feeding hole volume. An iterative scheme is used to simultaneously satisfy the equations of motion for the journal. The results presented include Bode plots of bearing-oscillation gain and phase for a particular bearing configuration for various combinations of parameters over a range of frequencies, including the resonant frequency.

NOMENCLATURE

a	Feeding hole diameter
c	Clearance between journal and sleeve
C_D	Discharge coefficient
e	Eccentricity
f_r	Resonant frequency
h	Film thickness
H	Dimensionless film thickness
k	Specific heat ratio
$\dot{m}_N$	Mass flow rate thru a feeding hole
$\dot{m}_\theta$	Mass flow rate in film of angular width $2\Delta\theta$
$\dot{M}$	Dimensionless mass flow rates
p	Film pressure
p_a	Ambient pressure
p_e	Exhaust pressure
p_N	Nozzle pressure
p_s	Supply pressure
P	Dimensionless pressure
R	Journal radius
R	Universal gas constant
t	Time
T	Temperature
w	Axial displacement of journal
W_o	Load supported by journal

x	Circumferential coordinate
z	Axial coordinate

Greek Symbols

α	Amplitude factor for angular vibration
β	Amplitude factor for radial vibration
δ	Perturbation factor
ε	Eccentricity ratio
μ	Dynamic viscosity of air
ω	Angular frequency of vibration
Λ	Bearing number
σ	Squeeze number
τ	Dimensionless time
θ	Dimensionless circumferential coordinate
ζ	Dimensionless axial coordinate (see Fig. 3 for location of ζ_1, ζ_2 and ζ_3)

Subscripts

0	Zeroth-order
1	First-order

Superscripts

'	Quantities within the region $\zeta_2 \leq \zeta \leq \zeta_3$ (outer bearing)
*	Value of amplitude factor as $\omega \to 0$

I. INTRODUCTION

There is currently considerable interest in gas bearing technology for application to rotating and reciprocating machinery for space-flight. Linear gas bearings have been proposed in Stirling cycle cryogenic cooler systems for infrared sensing satellites [1]. The bearings in these systems must allow long-term, noncontacting support of reciprocating components in the Stirling cooler. One such cooler design subjects a hydrostatic journal bearing to sinusoidal fluctuations in bearing exhaust pressure. The present paper focuses on an analysis of the static and dynamic characteristics of such pressure-excited bearings.

Of interest in the present research are the angular and radial forced vibration modes of a statically loaded, inherently compensated hydrostatic journal bearing due to oscillating exhaust pressures. The angular mode of vibration in the case of 180^{o} phase shift between exhaust pressures in a dual plane of feeding holes is depicted in Fig. 1a. Phase-shifted exhaust pressures can be physically achieved by segregating the exhaust systems of the two feeding planes as opposed to a common exhaust. The radial forced vibration mode of the above bearing when no phase shift is present is shown in Fig. 1b.

There are numerous analyses in the literature for various externally pressurized gas bearing systems. An excellent review of work up to 1969 is contained in the paper by Gross [2]. Majumdar [3] reviews the technology up to 1978. The citations compiled by

NITS [4,5] are a useful source of other material. Several authors [6,7,8,9,10,11] have analyzed the static and dynamic characteristics of inherently compensated bearings. Particularly noteworthy in this regard are the analyses of Lund [9,10] and of Majumdar [11] for orfice and inherently compensated externally pressurized journal bearings. Angular vibration or dynamic misalignment is discussed in only a limited number of papers [9,11,12,13]. The problem of oscillating exhaust or supply pressures seems to have escaped the attention of investigators entirely. Moreover, no linearized analyses have appeared which consider the case of vibration about an initially deflected journal position (caused by static loading).

The solution to the aforementioned problem of angular vibration with segregated phase-shifted oscillating exhausts is of particular importance since it has been identified as critical to the performance of such a bearing used to support the power piston of a candidate Stirling cooler design. It is therefore important to establish the static load-response characteristics, resonant frequencies and vibration amplitudes for the piston.

The theory developed in the present work is applied to a basic linear hydrostatic demonstration bearing designed by Mechanical Technology Incorporated (MTI) for NASA [14]. MTI conducted extensive proof-of-concept testing on this bearing configuration under steady pressurization. The present research will eventually use this same bearing in an experimental investigation of the dynamic effects studied analytically herein.

II. THEORY AND BASIC EQUATIONS

Governing Equations

The nondimensional Reynolds equation for the laminar, viscous gas film of the externally pressurized linear journal bearing shown in Fig. 2 is

$$\frac{\partial}{\partial\theta}\left(H^3\frac{\partial P^2}{\partial\theta}\right)+\frac{\partial}{\partial\zeta}\left(H^3\frac{\partial P^2}{\partial\zeta}\right)=2\sigma\frac{\partial(PH)}{\partial\tau}-\Lambda P\frac{\partial H}{\partial\zeta} \qquad (1)$$

for (P,P')

where $H = 1 + \varepsilon\cos\theta$

and where the nondimensional dependent and independent variables are as follows:

$$P=\frac{p}{p_a};\ H=\frac{h}{c}\quad \theta=\frac{x}{R};\ \zeta=\frac{z}{R};\ \tau=\omega t;\ \varepsilon=\frac{e}{c}$$

The bearing and squeeze number parameters are defined as

$$\Lambda=\frac{6\mu wR}{c^2p_a}\qquad \sigma=\frac{12\mu\omega R^2}{c^2p_a}$$

P is replaced by P' in the region $\zeta_2 \le \zeta \le \zeta_3$, and $\Lambda = 0$ in the present calculations.

Boundary Conditions

The boundary conditions which apply to equation (1) are as follows: From circumferential symmetry and continuity requirements, the boundary conditions in θ are

$$\frac{\partial P}{\partial\theta}(0,\zeta)=\frac{\partial P}{\partial\theta}(\pi,\zeta)=\frac{\partial P'}{\partial\theta}(0,\zeta)=\frac{\partial P'}{\partial\theta}(\pi,\zeta)=0 \qquad (2)$$

The boundary conditions in ζ are applied at the edges of the film $\zeta=\zeta_1$ and $\zeta=\zeta_3$, and at the plane of feeding holes $\zeta=\zeta_2$. For the oscillating exhaust pressure, the exhaust pressure oscillates at a fixed amplitude according to

$$P_e = 1 + \delta e^{i\tau} \tag{3}$$

and therefore, at the edge of the film

$$P(\theta,\zeta_1) = P'(\theta,\zeta_3) = 1 + \delta e^{i\tau} \tag{4}$$

At the plane of feeding holes the pressure is assumed continuous and consequently

$$P(\theta,\zeta_2) = P'(\theta,\zeta_2) \tag{5}$$

The remaining feeding plane boundary condition involves the derivatives of P and is different depending on whether the location considered is outside the feeding hole itself. Majumdar [11,15] has analyzed similar problems by a so called "point source" approach in which this distinction is clearly drawn. However, this approach also requires consideration of the two-dimensional Reynolds equation and a solution algorithm for it which is able to resolve spatial gradients over distances on the order of the hole diameter. Majumdar's work, as does the present research, utilizes a finite difference method with a grid size larger than that required for a true point source calculation. For this reason and because he does not consider the two dimensionality of the flow in the neighborhood of the feeding holes for the concentric journal [11], Majumdar's claims of a "point source" solution are

apparently exaggerated. In the present work, an additional approximate condition at the feeding hole plane consistent with the eventual discretization is obtained from requiring conservation of mass, i.e. requiring that the mass flow rate from each feeding hole (supply port) be equal to the mass flow rate into a segment of fluid film at that point. Effects due to the volume of the feeding hole are ignored.

The dimensionless expression for fully developed annular flow in a thin film of angular width $\Delta\Theta$ is, considering flow in both directions,

$$\dot{M}_\theta = \dot{m}_\theta \frac{24\mu T}{c^3 p_a^2} = \int_\theta^{\theta+\Delta\Theta} \left. \frac{\partial P^2}{\partial \zeta} \right|_{\zeta=\zeta_2} - \left. \frac{\partial P'^2}{\partial \zeta} \right|_{\zeta=\zeta_2} (1+\varepsilon\cos\theta^*)^3 \, d\theta^* \quad (6)$$

where $\dot{m}_\theta$ is the dimensional mass flow rate. The flow through the feeding holes (supply ports) is assumed adequately represented by one-dimensional isentropic flow with a discharge coefficient, C_D, and effective dimensionless back pressure, P_N. There is some controversy regarding the adequacy of this kind of a nozzle flow model for gas bearings due to effects from pressure recovery and peaking in pressure around the discrete feeding holes. In the present work C_D is regarded as an empirical constant which can be adjusted slightly to partially compensate for these effects as well as nozzle losses so as to produce results acceptable for design purposes. A more significant correction for the peaking phenomenon is described later.

The strip of angular width $\Delta\Theta$ in equation (6) is associated

with the flow emanating from a single hole, i.e. it is the angular distance between dividing streamlines at $\zeta=\zeta_2$. Therefore, the additional boundary relation required can be obtained from conservation of mass by equating the dimensional expression for isentropic mass flow from a single feeding port, $\dot{m}_N$ to $\dot{m}_\theta$, and connecting P_N to $P(\theta,\zeta_2)$. The simplest such assumption connection the nozzle exit pressure, P_N to the film pressure, $P(\theta,\zeta)$ is that $P_N=P(\theta_{hole},\zeta_2)$. However, as mentioned previously, the approximate numerical procedure to be discussed in the next section is not able to completely resolve pressure peaking in the vicinity of the discrete feeding hole. Therefore, at the boundary an equivalent line source boundary condition is introduced which is assumed to reproduce the effect of the discrete holes on the flow field remote from the holes. J. Lund [10] developed an empirical correction relating the nozzle exit pressure to the equivalent line source film pressure in the vicinity of the feeding holes for equivalent mass flow. The correction as recommended in [16] is

$$P_N = AP(\theta_{hole},\zeta_2) \; ; \quad A = 1.5 \tag{7}$$

Majumdar [3] has been critical of such an approach and discusses its pitfalls. Also there may be further dangers for the present dynamic work, since the correction was developed for static calculations. Nevertheless, because of its simplicity, it was chosen for the present calculations. Majumdar's point source method [15] does not seem to be a viable alternative unless significant computing resources are allocated to performing computations on a dense grid;

thereby allowing the steep flow gradients in the neighborhood of the feeding holes to be resolved. The relation derived from conservation of mass and equation (7) contains the pressure implicitly and is nonlinear. An iterative scheme is necessary to apply it as a boundary condition in the numerical solution.

III. APPLICATION OF PERTURBATION THEORY

Perturbation Equations

A conventional perturbation method, assuming sinusoidal response to a small sinusoidal excitation is used to simplify the governing equations. In applying the method, it is assumed that

$$P = P_0 + P_1\,\delta e^{i\tau} \quad \text{and} \quad H = H_0 + H_1\,\delta e^{i\tau}$$

where

$$H_0 = 1 + \varepsilon_0 \cos\theta \quad \text{and} \quad H_1 = (\zeta A\alpha + \beta)\cos\theta$$

α,β and $P_1(\theta,\zeta)$ are, in general, complex to reflect phase shifts from the driving pressure. $\delta\alpha$ and $\delta\beta$ are the amplitudes of the angular and radial displacements respectively of the vibration modes shown in Figs. 1(a) and (b). Although coupled angular and radial vibration will not be considered in the present calculations, the differential equation for the perturbation quantities were derived for this general case. Expanding equation (3), the resulting perturbation equations are for $\delta << 1$

$O(\delta^0)$

$$\frac{\partial}{\partial\theta}\left(H_0^3\,\frac{\partial P_0^2}{\partial\theta}\right) + H_0^3\,\frac{\partial^2 P_0^2}{\partial\zeta^2} = 0 \qquad (8)$$

$O(\delta^1)$

$$\frac{\partial}{\partial\theta}\left(H_0^3\,\frac{\partial Q}{\partial\theta}\right) + H_0^3\,\frac{\partial^2 Q}{\partial\zeta^2} - i\sigma H_0\,\frac{Q}{P_0} =$$

$$- \frac{3}{2} H_0^2(\zeta A\alpha+\beta)\cos\theta \frac{\partial^2 P_0^2}{\partial \zeta^2} - \frac{3}{2} H_0^2 A\alpha\cos\theta \frac{\partial P_0^2}{\partial \zeta} - \frac{3}{2} H_0^2(\zeta A\alpha+\beta)\cos\theta \frac{\partial^2 P_0^2}{\partial \theta^2}$$

$$- \frac{3}{2} \frac{\partial}{\partial \theta} [H_0^2(\zeta A\alpha+\beta)\cos\theta] \frac{\partial P_0^2}{\partial \theta} - \Lambda A\alpha\cos\theta P_0 + i\sigma (\zeta A\alpha+\beta)\cos\theta P_0 \qquad (9)$$

where

$$Q = P_0 P_1 \text{ and } A = R/c$$

In the above equations, it should be noted that symmetry requires that $P_0(\theta,\zeta) = P'_0(\theta,\zeta)$ and that equation (9) applies also to $Q' = P_0 P'_1$.

Perturbation Boundary Conditions

The circumferential boundary conditions are straightforward. For the zeroth-order differential equation, from equation (2) the expansion gives

$$\frac{\partial P_0}{\partial \theta}(0,\zeta) = \frac{\partial P_0}{\partial \theta}(\pi,\zeta) = \frac{\partial P'_0}{\partial \theta}(0,\zeta) = \frac{\partial P'_0}{\partial \theta}(\pi,\zeta) = 0 \qquad (10)$$

Also from the expansion of equation (2) the first order boundary condition is

$$\frac{\partial Q}{\partial \theta}(0,\zeta) = \frac{\partial Q}{\partial \theta}(\pi,\zeta) = \frac{\partial Q'}{\partial \theta}(0,\zeta) = \frac{\partial Q'}{\partial \theta}(\pi,\zeta) = 0 \qquad (8)$$

At the edge of the film the zeroth-order condition is from expansion of equation (4)

$$P_0(\theta,\zeta_3) = P'_0(\theta,\zeta_3) = 1 \qquad (9)$$

Similarly from equation (4) the first-order condition is

$$Q(\theta,\zeta_3) = Q'(\theta,\zeta_3) = 1 \qquad (10)$$

The boundary condition at $\zeta=\zeta_2$ is a bit more involved, especially for the first-order equation.

In the numerical analysis to be discussed in the next section, each feeding hole (supply port) is associated with a strip of width $\Delta\Theta = 2\Delta\theta$ where $\Delta\theta$ is the angular grid interval in the circumferential direction; therefore, from equation (6)

$$\dot{m}_\theta = \frac{c^2 p_a}{24\mu RT}\left(\frac{\partial P^2}{\partial\zeta}\bigg|_{\zeta=\zeta_2} - \frac{\partial P'^2}{\partial\zeta}\bigg|_{\zeta=\zeta_2}\right)H^3\ \frac{2}{N\pi} \qquad (11)$$

This equation represents the mass flow rate through an element of the film of angular width $2\pi/N = 2\Delta\theta$, where N is the number of holes (there are two grid intervals corresponding to each hole). The equation is applied assuming H, $\partial P^2/\partial\zeta$ and $\partial P'^2/\partial\zeta$ are not functions of θ over the width of the film; they are evaluated at the mid point of the interval $2\Delta\theta$, i.e. at the hole.

The mass flow rate through the supply ports is given by

$$\dot{m}_N = \frac{\pi a c p_a}{(RT)^{1/2}} C_D\ \phi\ H \qquad (12)$$

where

$$\phi = \left(\frac{P_N}{P_s}\right)^{1/k}\left[1-\left(\frac{P_N}{P_s}\right)^{\frac{k-1}{k}}\right]^{1/2}\left(\frac{2k}{k-1}\right)^{1/2} P_s$$

or if the flow is choked

$$\phi = \left(\frac{2k}{k-1}\right)^{1/2}\left(\frac{2}{k+1}\right)^{\frac{1}{k-1}} P_s$$

ϕ must be converted to a linear approximation in order for the expansion technique to work. Recall that P_N is related to the film pressure by equation (7). Linearizing ϕ in a Taylor series expansion and making the necessary substitutions, equation (12) becomes

$$\dot{m}_N = \frac{\pi a c}{(RT)^{1/2}} C_D \left[\phi(P_s, P_N(P_0)) + \left.\frac{\partial \phi}{\partial P_N}\right|_{P_N=P_N(P_0)} \frac{AQ}{P_0}\delta e^{i\tau}\right] H \qquad (13)$$

Expanding equation (11), equating it to equation (13), and invoking symmetry, the zeroth-order boundary condition at the holes in the feeding plane is

$$\frac{\partial P_0^2}{\partial \zeta} = \frac{\eta/2\phi(P_s, P_N(P_0))}{(1+\varepsilon\cos\theta)^2} \qquad (14)$$

where the feeding parameter,

$$\eta = \frac{12\mu(RT)^{1/2} a\, C_D\, N}{c^2 p_a}$$

The boundary condition described by equation (14), is nonlinear as well as implicit and therefore an iterative scheme must be used in applying it.

In addition to the condition of equation (14), a further condition from the expansion of equation (5) is

$$P_0(\theta,\zeta_2) = P'_0(\theta,\zeta_2) \tag{15}$$

The first-order condition at the feeding plane obtained from equating the expanded form of equation (11) with equation (13) is

$$\left.\frac{\partial Q}{\partial \zeta}\right|_{\zeta=\zeta_2} - \left.\frac{\partial Q'}{\partial \zeta}\right|_{\zeta=\zeta_2} = \frac{n/2}{(1+\varepsilon\cos\theta)^2} \left.\frac{\partial \phi}{\partial P_N}\right|_{P_N=P_N(P_0)} \left[\frac{AQ}{P_0} - \frac{2H_1}{H_0}\frac{\partial P_0^2}{\partial \zeta}\right] \tag{16}$$

Although this condition is linear, it is implicit in Q since it contains both Q and Q' and therefore must,as equation (14),be applied in an iterative fashion.

The remaining condition to be satisfied at the feeding plane is obtained from the expansion of

$$Q(\theta,\zeta_2) = Q'(\theta,\zeta_2) \tag{17}$$

Although the derivative boundary conditions, equations (14) and (16) were derived for a point located at the center of a hole, by interpolating between the hole locations an approximate derivative condition can be obtained for any point along the circumference in the feeding plane.

IV. EQUATIONS OF MOTION

The steady load supported by the bearing, W_0 can be computed from integrating the distribution of P_0. It is

$$-\frac{W_0}{R^2 p_a} = 8 \int_0^{\pi} \int_{\zeta_1}^{\zeta_2} P_0 \cos\theta d\zeta d\theta \tag{18}$$

For linear motion with dimensionless amplitude factor β about the equilibrium position ε_0, the displacement is

$$y = c\beta\delta e^{i\tau} \tag{19}$$

and the equation of motion for a journal of mass, m, supported in two places by two physically separate bearings with separate feeding planes as in Fig. 1 is

$$m\frac{d^2y}{dt^2} = -2Fe^{i\tau} \tag{20}$$

Hence, substituting equation (19) into equation (20)

$$\beta = -\frac{2F}{\delta m\omega^2 c} \tag{21}$$

where F, the amplitude of the dynamic restoring force due to the pressure in the fluid film is computed from

$$-\frac{F}{R^2 p_a} = 2\delta \int_0^{\pi} \int_{\zeta_1}^{\zeta_2} P_1 \cos\theta d\zeta d\theta + 2\delta \int_0^{\pi} \int_{\zeta_2}^{\zeta_3} P' \cos\theta d\zeta d\theta \tag{22}$$

and therefore from equations (21) and (22)

$$\beta = \frac{4R^2 p_a}{m\omega^2 c}\left[\int_0^{\pi} \int_{\zeta_1}^{\zeta_2} P_1 \cos\theta d\zeta d\theta + \int_0^{\pi} \int_{\zeta_2}^{\zeta_3} P' \cos\theta d\zeta d\theta\right] \tag{23}$$

Similarly for angular motion about $\zeta = 0$, the angular displacement Ψ, with amplitude factor α is

$$\Psi=\alpha\delta e^{i\tau} \tag{24}$$

and employing the angular equation of motion for a configuration with two feeding planes as in Fig. 1, symmetry about $z = 0$, and a mass moment of inertia, I the angular equivalent to equation (23) is

$$\alpha = \frac{4R^3 p_a}{I\omega^2}\left[\int_0^{\pi}\int_{\zeta_1}^{\zeta_2} P_1\,\zeta\cos\theta\,d\zeta\,d\theta + \int_0^{\pi}\int_{\zeta_2}^{\zeta_3} P'_1\,\zeta\cos\theta\,d\zeta\,d\theta\right] \tag{25}$$

Equations (18), (23) and (25) together with the perturbation differential equations, equations (8) and (9) and their associated boundary conditions constitute a completely closed set of equations for determining the response of the bearing system to oscillating exhaust pressure in the modes illustrated in Fig. 1.

V. NUMERICAL METHOD

Zeroth Order Solution

For a given eccentricity ϵ_0, the zeroth order perturbation equation, equation (8) with its associated boundary conditions can be solved for the unknown pressure distribution.

To solve the perturbation equations numerically, the bearing film is discretized as shown in Fig. 3. The choice of the grid shown was somewhat arbitrary but seemed to be a good compromise between the resolution required and economy. The moderate angular variation of pressure computed for the cases studied did not seem to warrant further grid reduction in the angular direction; the sufficiency of the axial grid was tested by comparing results obtained from two different axial grid distributions.

Central differencing is applied to obtain finite difference approximations for the zeroth-order equation. Solution of the resulting difference equations with their numerical boundary conditions are routine with the exception of the treatment of the feeding plane boundary. As mentioned in the preceding section, an iterative solution of the system of zeroth-order equations is needed to satisfy the feeding plane boundary condition at $\zeta=\zeta_2$. A Newton-Raphson scheme iterates on each unknown feeding hole pressure by comparing zeroth-order flow rates through the feeding holes with those obtained from solution of the finite difference equations for the zeroth-order film pressure and updating the pressures until convergence is achieved.

Since the solution to the present problem actually requires obtaining the eccentricity ε_0 for a known load W_0 a second iterative procedure is applied,calculating the W_0 corresponding to a series of ε_0's until the known value is obtained.

Details of all the iteration and differencing techniques are given in [17].

First-Order Solution

With the real zeroth-order solution having been determined, the solution to the complex first-order equation, equation (9) and consequently the complex amplitudes of angular and radial vibration can be obtained. As in the case of the zeroth-order differential equation, central finite difference approximations are used for the first-order equation, equation (9).

In obtaining the first-order solution, the equations of motion, equations (23) and (25) must be solved simultaneously with equation (9). To accomplish this a tentative valve of α (or β) is used in equations (9) and (16) to obtain a distribution of Q which is then integrated using equation (25) (or (23)) to compute α (or β). Employing a Newton-Raphson iteration scheme, the computed and tentative values are compared to update the tentative value. Convergence is achieved when the tentative and computed values agree. The iteration process is also used to transform the implicit boundary conditions, equations (16) and (17) into explicit boundary conditions by lagging $\partial Q'/\partial \zeta$ one iteration behind.

Details of the solution procedure, including the finite-difference equations, are given in [17].

VI. RESULTS AND DISCUSSION

In performing the present computations, two journal masses were considered; one with mass equivalent to the MTI journal [14] and one with additional mass added to reduce the resonant frequency for future experimental purposes. The mass of the unmodified and the weighted MTI journal were taken to be 2.7 and 5.4 kilograms (6 and 12 pounds) with mass moments of inertia of 2.04×10^{-5} kg-m^2 and 4.27×10^{-5} kg-m^2 respectively. The two bearing surfaces which support the journal, each with twelve centrally-located feeding holes were 0.0254 meters (1 in.) wide. The feeding hole diameters were 0.000889 meters (0.035 in) and the bearing diameter was 0.0508 meters (2 in.)with a clearance of 1.778×10^{-5} meters (0.0007 in.). The three values for the supply pressure, for which static (zeroth-order) results will be presented, correspond to the pressures used by MTI [13] in their experiments. However, a different set of supply pressures was selected for the dynamic results because of limitations in the eventual dynamic experiments to be performed.

Zeroth-Order Results

For each of the three values of supply pressure referred to earlier, the zeroth-order pressure distribution and subsequently the static load, W_0 were calculated for several journal deflections. The results depicted in Fig. 4 are compared to the experimental and theoretical results obtained by MTI [14]. As mentioned in Section II, C_D is adjusted to produce overall results acceptable for design purposes.

After comparing results obtained for several round number values of C_D in a physically realistic range, it was determined that a C_D equal to 0.7 gives good results when all three supply pressures are considered. No further optimization was attempted since the approximate nature of the analysis does not warrant it. From Fig. 4 it appears that the present theory is a slight improvement over the MTI static deflection theory, considering all three supply pressures. This improvement can be attributed to the more detailed modeling in the present work which considers effects such as circumferential interaction between the flow from individual holes, which is not included in the MTI theory.

First-Order Results

The first-order calculations are intended to show the dynamic response of the journal to oscillating exhaust pressure including the location of resonant frequencies. Computations were performed for both vibrational modes depicted in Fig. 1. Results were obtained showing the effects of variations in the supply pressure, journal mass or moment of inertia, and configuration dependent changes in squeeze number and feeding parameter. The range of vibrational frequencies analyzed was from 1 to 1000 Hz. The three values considered for the supply pressure were 3.8×10^5, 5.1×10^5 and 6.9×10^5 N/m^2.

Table 1 summarizes the significant input and computed parameters for the angular vibrational mode. In the table α^* indicates the

value of α as ω approaches zero. The factors multiplying the squeeze number and feeding parameter indicate cases computed for hypothetical configuration changes by substituting effective values of these parameters in the governing equations which were in turn, one-tenth and ten times the actual values of these parameters obtained from the present bearing system physical constants. Stable solutions were found for all cases computed.

For application to reciprocating mechanical cooler components, the vibrational frequency of interest is around 30 Hz and the supply pressure is about 3.8×10^5 N/m^2. Therefore from Table 1, it is obvious that for most cases in the cooler application there is little resonance effect. This is also borne out by examination of Figs. 5 and 6 which are Bode plots of gain versus frequency parameter, illustrating the effects of supply pressure and journal mass moment of inertia respectively on the frequency response of the journal in the angular mode. It is also interesting to note from these figures and Table 1 that at the low frequencies of interest the amplitude of angular displacement increases with increasing supply pressure and journal mass moment of inertia. As anticipated, the results show that lowering the supply pressure and increasing the mass moment of inertia reduce the resonant frequencies. Should the supply pressure in the space cooler application be reduced much below 3.8×10^5 N/m^2, resonant effects will be significant at 30 Hz.

Finally, it can also be demonstrated that, for the cases of interest, the results as summarized in Table 1 indicate that journal

TABLE 1 Input and computed parameters for angular vibration with oscillating exhaust pressure

I ($kg\text{-}m^2$)	p_s (N/m^2)	η_{eff}	σ_{eff}	α^*	f_r (Hz)
2.0×10^{-5}	3.8×10^{5}	η	σ	0.116×10^{-3}	72
2.0×10^{-5}	5.1×10^{5}	η	σ	0.252×10^{-4}	100
2.0×10^{-5}	6.9×10^{5}	η	σ	0.735×10^{-5}	125
4.3×10^{-5}	3.8×10^{5}	η	σ	0.317×10^{-3}	42
4.3×10^{-5}	5.1×10^{5}	η	σ	0.530×10^{-4}	68
4.3×10^{-5}	6.9×10^{5}	η	σ	0.147×10^{-4}	88
2.0×10^{-5}	5.1×10^{5}	η	0.1σ	0.252×10^{-4}	100
2.0×10^{-5}	5.1×10^{5}	η	10σ	0.252×10^{-4}	115
2.0×10^{-5}	5.1×10^{5}	0.1η	σ	0.101×10^{-4}	122
2.0×10^{-5}	5.1×10^{5}	10η	σ	0.913×10^{-4}	42
$\eta = 14.5455$					

TABLE 2 Input and computed parameters for radial vibration with oscillating exhaust pressure

m (kg)	p_s (N/m^2)	η_{eff}	σ_{eff}	β^*	f_r (Hz)
2.7	3.8×10^5	η	σ	0.796×10^{-1}	430
2.7	5.1×10^5	η	σ	0.181×10^{-1}	575
2.7	6.9×10^5	η	σ	0.535×10^{-2}	715
5.4	3.8×10^5	η	σ	0.201×10^{0}	285
5.4	5.1×10^5	η	σ	0.377×10^{-1}	400
5.4	6.9×10^5	η	σ	0.106×10^{-1}	505
2.7	5.1×10^5	η	0.1σ	0.181×10^{-1}	560
2.7	5.1×10^5	η	10σ	0.181×10^{-1}	660
2.7	5.1×10^5	0.1η	σ	0.745×10^{-2}	665
2.7	5.1×10^5	10η	σ	0.449×10^{-1}	270
$\eta = 14.5455$					

contact with the sleeve of the MTI bearing will not occur if the bearing is subjected to low-frequency oscillating exhaust pressures in the range even marginal application of pertubation theory, i.e. for $\delta < 1$.

Table 2 summarizes the significant input and computed parameters for the radial vibration mode. The vibrational amplitudes are less than in the angular mode. The resonant frequencies computed differ somewhat from the classical results based on static stiffness due to the squeeze and compressibility effects described in early work by Mullan and Richardson [6]. Figure 7 is a Bode plot illustrating the effect of supply pressure on frequency response for the radial mode. The trends shown in the radial results are essentially those observed in the angular results.

VII. SUMMARY AND CONCLUSIONS

The results presented herein indicate that classical pertubation theory gas bearing analysis can be successfully applied to predict the dynamic response of statically-loaded inherently compensated hydrostatic gas bearings to oscillating exhaust pressures for both angular and radial vibration modes. The method developed uses a line source approximation with a mass flow correction factor in the numerical analysis. The resolution needed for a true point source calculation would require excessively large finite difference grid line densities.

The static calculations show good agreement with experiment and previous theoretical work. The dynamic calculations indicate that the bearing configuration of interest does not approach resonant conditions or contact the sleeve. Further, the amplitude of displacement increases with increasing journal mass and supply pressure, and is greater for angular than for radial vibration. Experimental work is in progress to verify the numerical results. Experimental confirmation is especially needed to support the results of the dynamic calculations.

ACKNOWLEDGEMENT

This research was supported, in part, by the National Aeronautics and Space Administration.

REFERENCES

1. Sherman, A., "Cryogenic Cooling for Space Sensors, Instruments, and Experiments," Astronautics and Aeronautics, Vol. 16, 1978, pp. 39-47.

2. Gross, W.A., "A Review of Developments in Externally Pressurized Gas Bearing Technology since 1959," Journal of Lubrication Technology, Vol. 91, No. 1, 1969, pp. 161-167.

3. Majumdar, B.C., "Externally Pressurized Gas Bearings: A Review," Wear, Vol. 62, 1980, pp. 299-314.

4. National Technical Information Service, Gas Bearing, Volume 2- Citations from the NTIS Data Base, NTIS/PS-78/1278, Springfield, Virginia, 1978.

5. National Technical Information Service, Gas Bearings - Citations from the Engineering Index Data Base, NTIS/PS-78/1278, Springfield, Virginia, 1978.

6. Mullan, P.J., and Richardson, H.H., "Plane Vibration of the Inherently Compensated Gas Journal Bearing; Analysis and Comparison with Experiment," ASLE Transactions, Vol. 7, 1964, pp. 277-287.

7. Stiffler, A.K. "Analysis of the Stiffness and Damping of an Inherently Compensated, Multiple-Inlet, Circular Thrust Bearing," Journal of Lubrication Technology, Vol. 7, 1964, pp. 379-437.

8. Stiffler, A.K., and Smith, D.M., "Dynamic Characteristics of an Inherently Compensated, Square, Gas Film Bearing," Journal of Lubrication Technology, Vol. 97, No. 1, 1975, pp. 52-62.

9. Lund, J.W., "The Hydrostatic Gas Journal Bearing with Journal Rotation and Vibration," Journal of Basic Engineering, Vol. 2, No. 2, 1964, pp. 328-336.

10. Lund, J.W., "A Theoretical Analysis of Whirl Instability and Pneumatic Hammer for a Rigid Rotor in Pressurized Gas Bearings," Journal of Lubrication Technology, 1967, pp. 154-166.

11. Mujumdar, B.C., "Dynamic Behavior of Externally Pressurized Gas Journal Bearings with Multiple Supply Holes," Wear, Vol. 34, 1975, pp. 189-199.

12. Rao, N.S., "Tilt Stiffness and Damping of Externally Pressurized Pourous Gas Journal Bearings," Wear, Vol. 47, 1978, pp. 31-44.

13. Rao, N.S., "Analysis of Dynamic Tilt Stiffness and Damping Coefficients of Externally Pressurized Pourous Gas Journal Bearings," Wear, Vol. 47, 1978, pp. 359-363.

14. McCormick, J. "Performance Demonstration Under Air Operation of a Reciprocating Hydrostatic Gas Bearing for a Stirling Cycle Cryogenic Cooler," MTI 80TR11, 1979, Mechanical Technology Incorporated, Latham, New York.

15. Mujumdar, B.C., "On the General Solution of Externally Pressurized Gas Journal Bearings," Journal of Lubrication Technology, October 1972, pp. 291-296.

16. Mechanical Technology Incorporated, "Design of Gas Bearings," Vol. 1, 1972, Sec. 5.5.

17. Branch, H.D., "Static and Dynamic Characteristics of Linear Hydrostatic Gas Bearings, M.S. Thesis, Department of Mechanical Engineering, Howard University, Washington, D.C., July 1982.

FIGURE CAPTIONS

Figure 1 — Modes of vibration due to oscillating supply or oscillating exhaust pressure

Figure 2 — Bearing geometry and coordinate system

Figure 3 — Grid for finite difference approximations

Figure 4 — Load versus eccentricity curves

Figure 5 — Effect of supply pressure on frequency response for angular vibration with oscillating exhaust ($I = 2.04 \times 10^{-5}$ kg-m^2)

Figure 6 — Effect of mass moment of inertia on frequency response for angular vibration with oscillating exhaust ($p_s = 3.8 \times 10^5$ N/m^2)

Figure 7 — Effect of supply pressure on frequency response for radial vibration with oscillating exhaust ($m = 2.7$ kg)

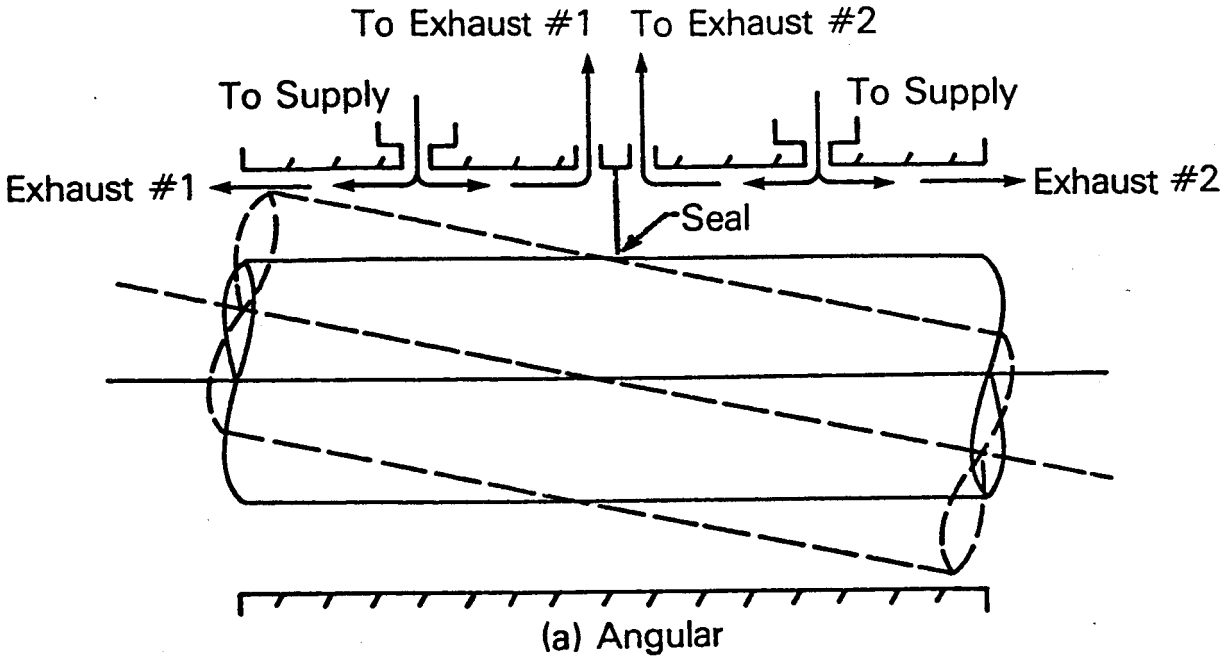

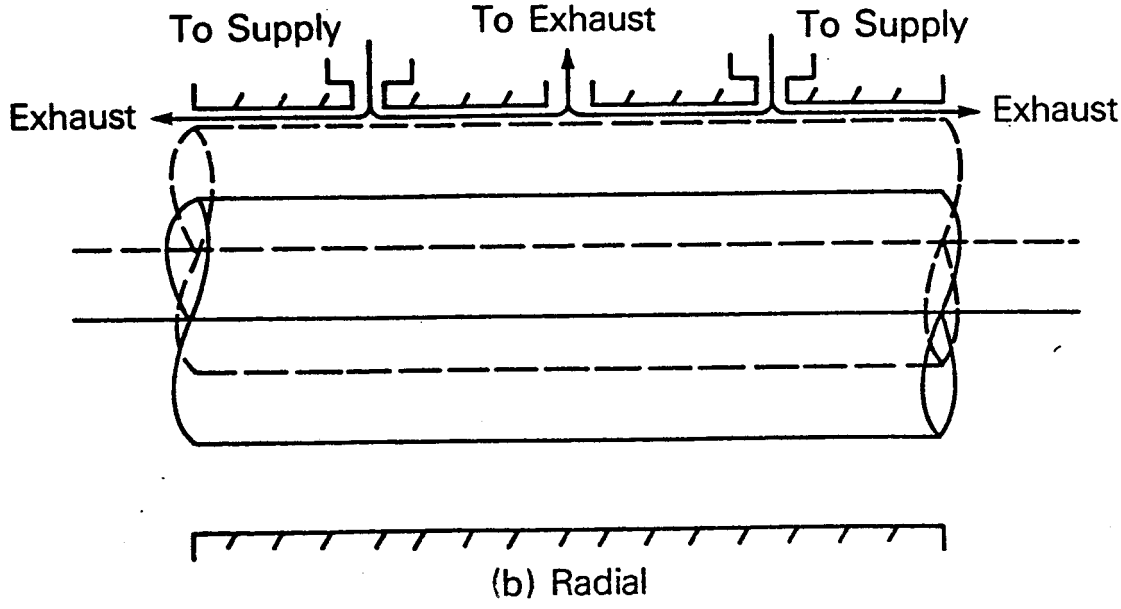

Fig. 1 Modes of vibration due to oscillating supply or oscillating exhaust pressure

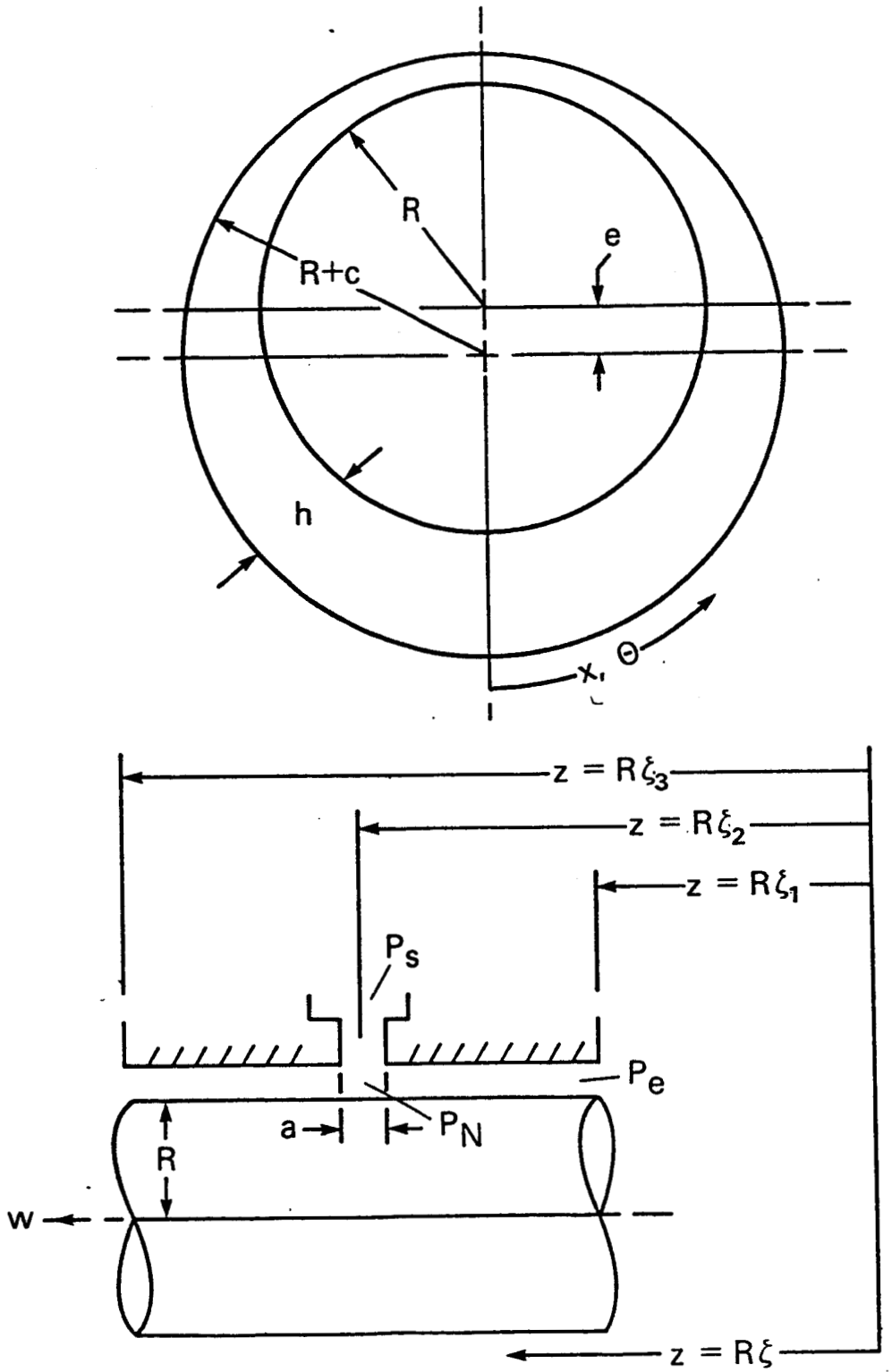

Fig. 2 Bearing geometry and coordinate system

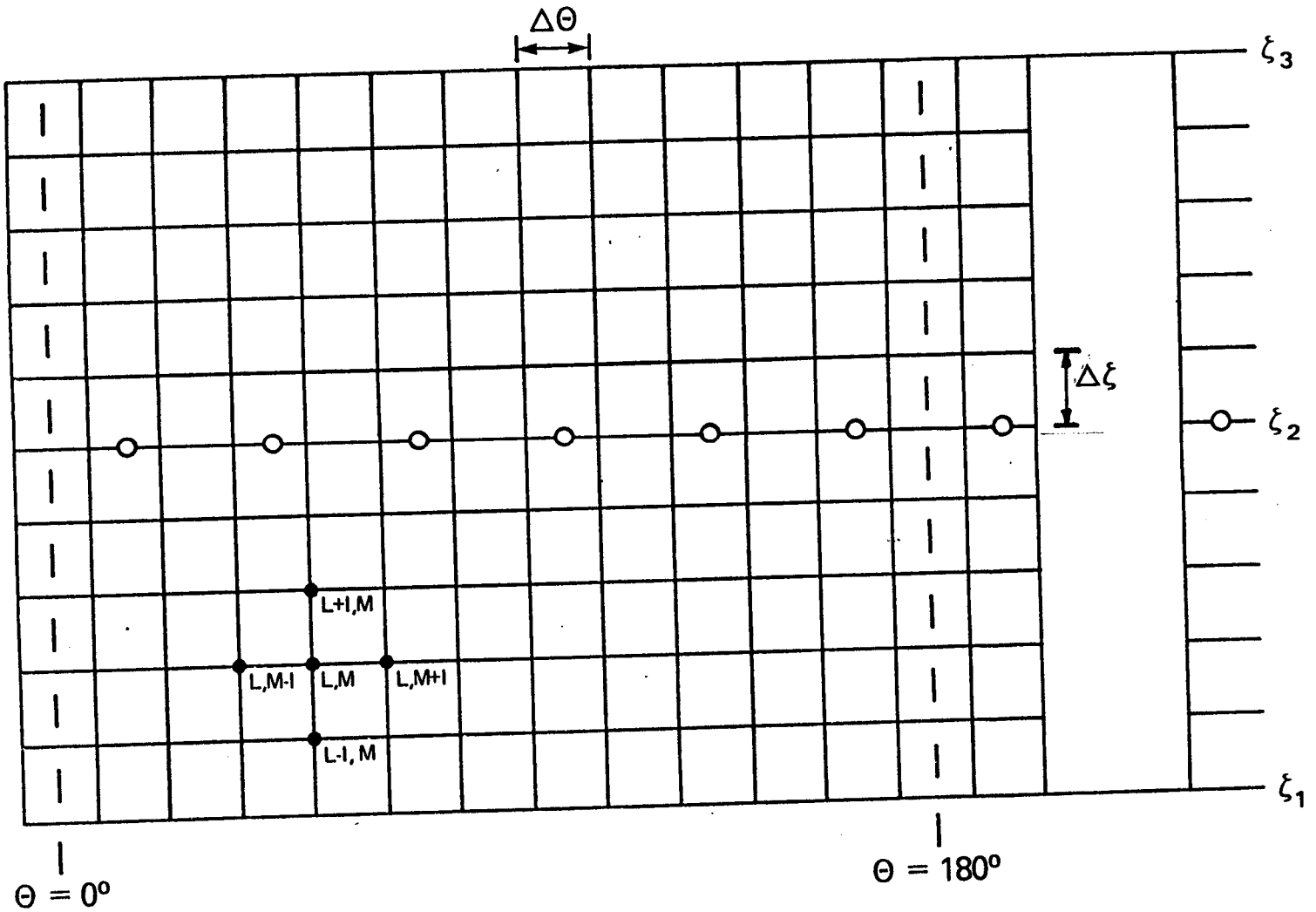

Fig. 3 Grid for finite difference approximations

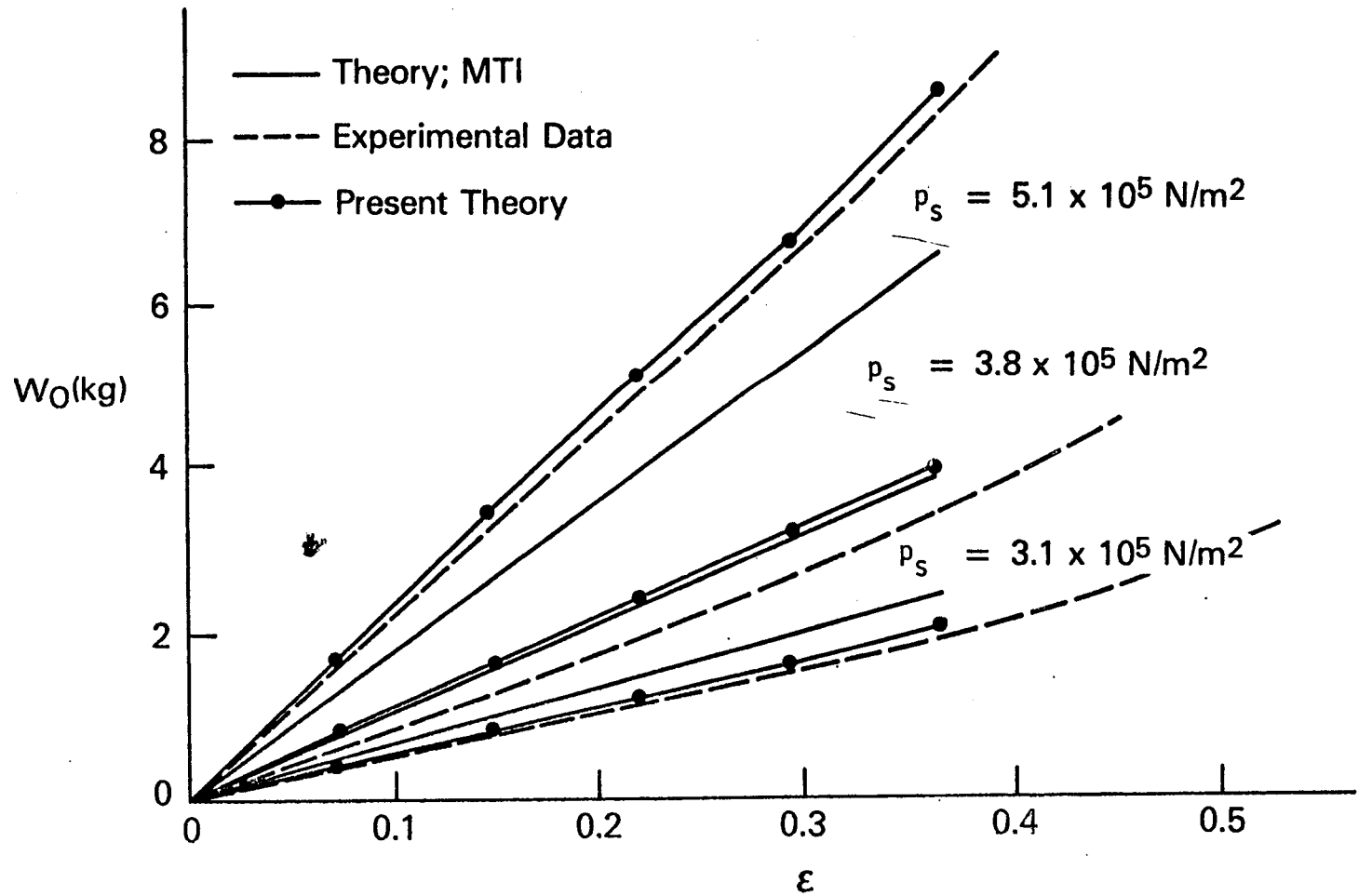

Fig. 4 Load versus eccentricity curves

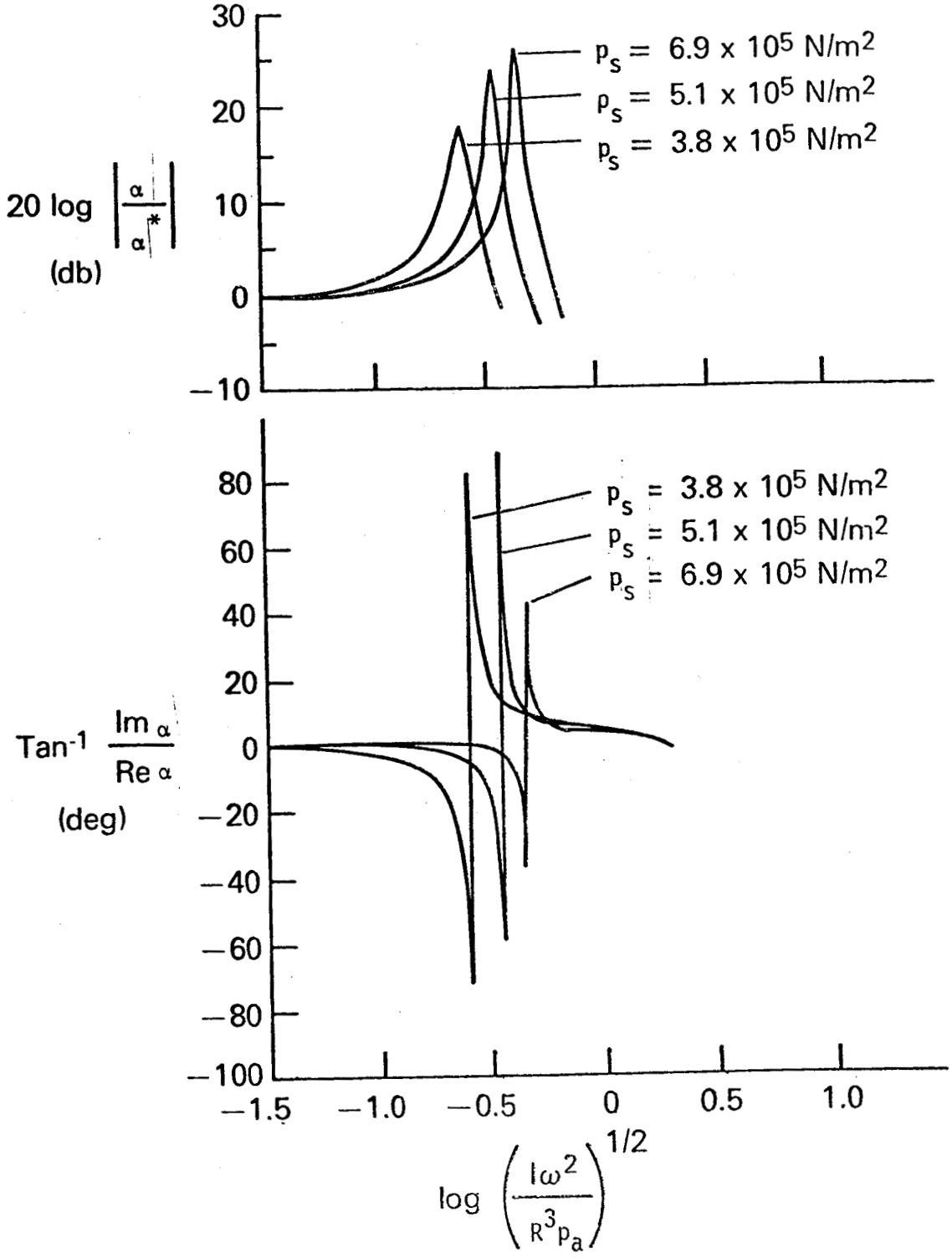

Fig. 5 Effect of supply pressure on frequency response for angular vibration with oscillating exhaust ($I = 2.04 \times 10^{-5}$ kg-m^2)

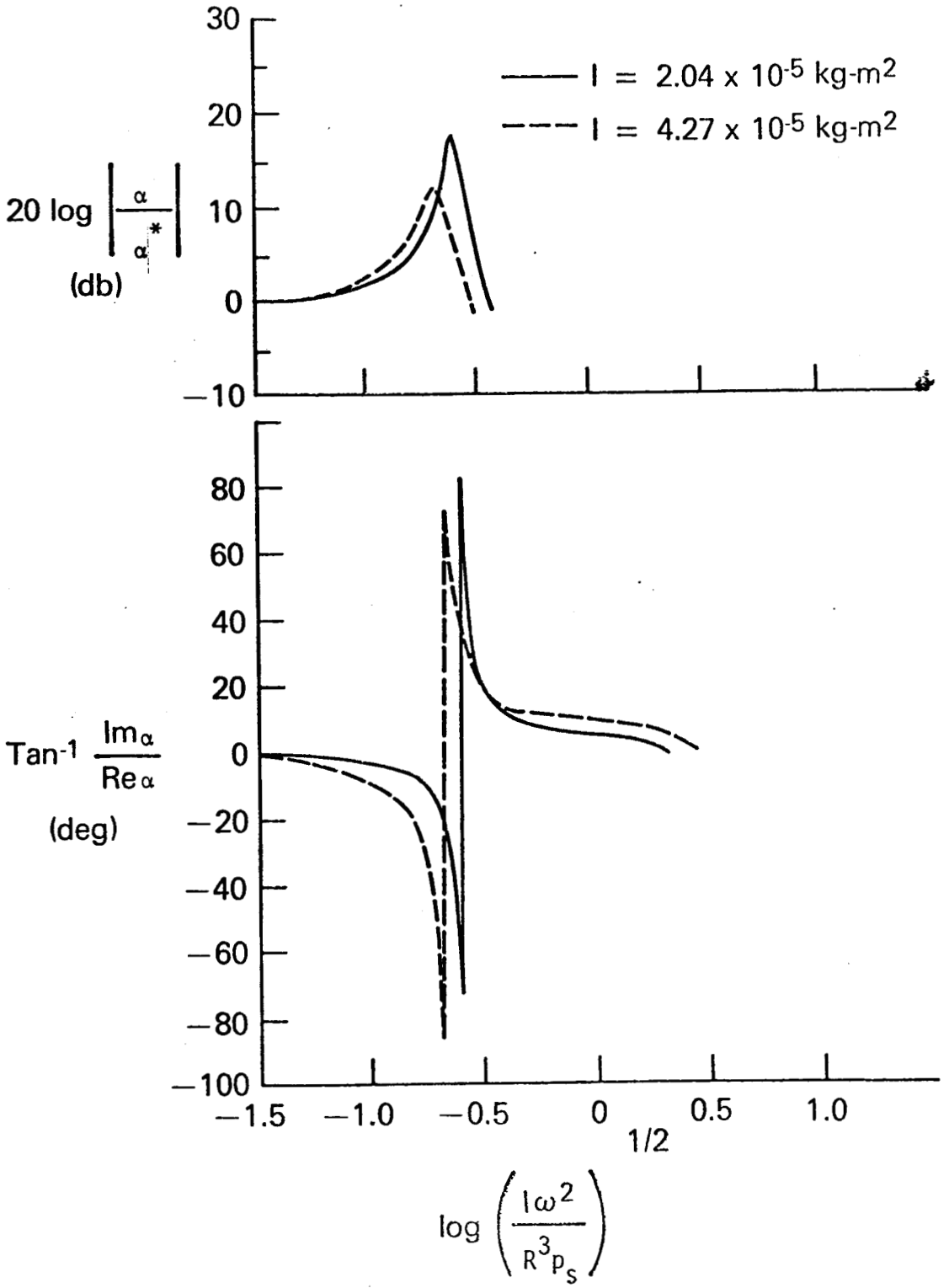

Fig. 6 Effect of mass moment of inertia on frequency response for angular vibration with oscillating exhaust (p_s = 3.8x10^5 N/m^2)

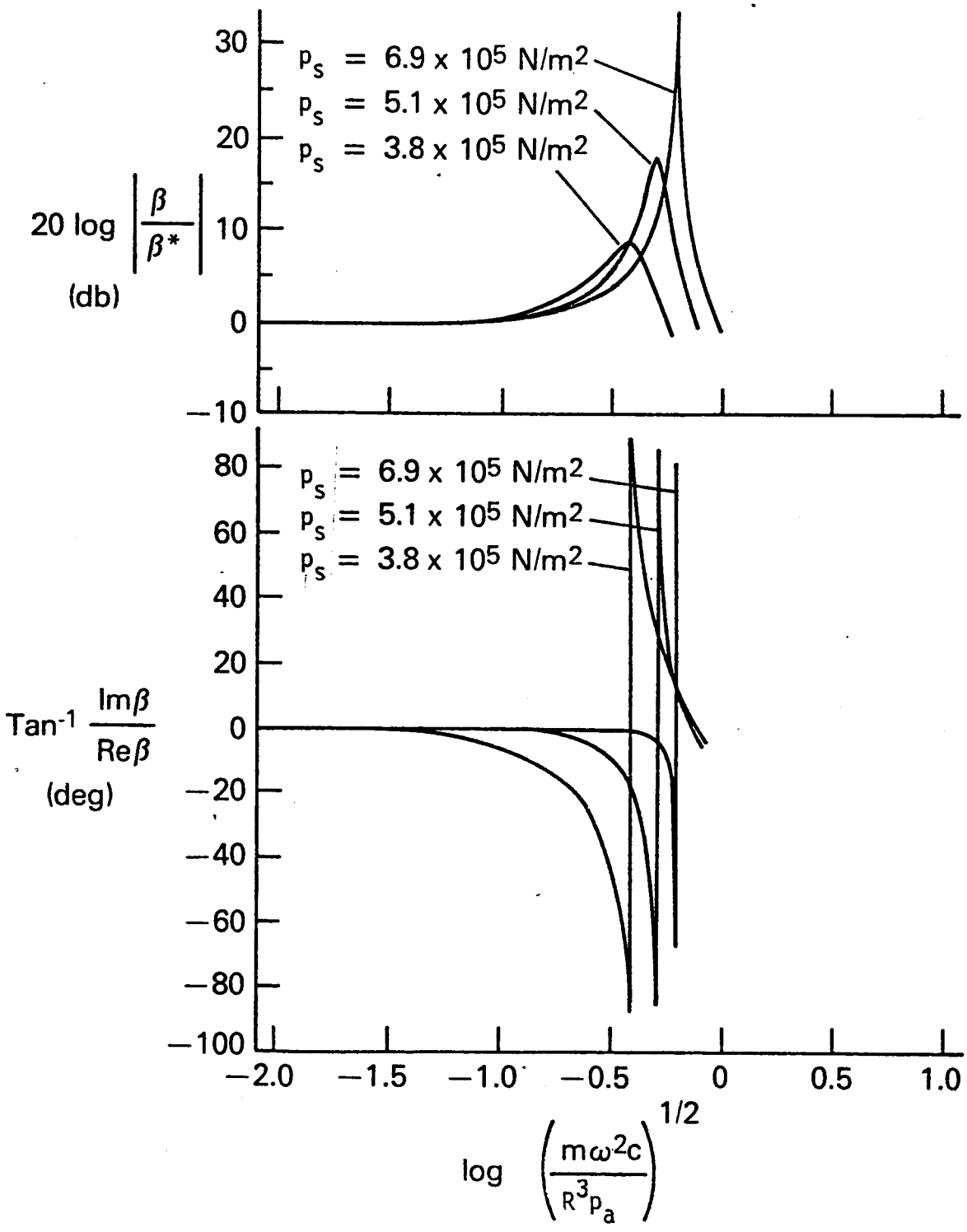

Fig. 7 Effect of supply pressure on frequency response for radial vibration with oscillating exhaust (m = 2.7 kg)